ISSN 2079-1704. Хімія, фізика та технологія поверхні. 2023. Т. 14. № 2. С. 159-172

PACS 31.15.E−; 82.65.+r doi: 10.15407/hftp14.02.159

D.M. Mamand, H.M. Qadr

QUANTUM COMPUTATIONS AND DENSITY FUNCTIONAL THEORY ON CORROSION INHIBITION EFFICIENCY OF BIA, HBT, MBI AND PIZ COMPOUNDS

University of Raparin, College of Science, Department of Physics
Sulaymaniyah, 46012, Iraq, E- mail: hiwa.physics@uor.edu.krd

This study determined the corrosion inhibition levels of benzimidazole (BIA), 1-hydroxybenzotriazole (HBT), methylbenzimidazole (MBI) and 4-phenylimidazole (PIZ). By using simulation, it was possible to have a complete relationship with the experimental work because the results were completely consistent. Density functional theory (DFT) and Monte Carlo simulations were used to calculate several quantum chemical parameters. The molecules are simulated using quantum chemical calculations with Gaussian09 software. Fundamental factors determining the corrosion order of molecules are the highest-energy occupied and lowest-energy unoccupied molecular orbitals (HOMO and LUMO), frontier molecular orbital energy, back donating energy, electrophilicity, nucleophilicity, energy gap ΔE, absolute electronegativity (χ), softness, the number of electrons (ΔN) transferred from inhibitors to iron, the dipole moment (μ), the global hardness (η) and the total energy.

Keywords*: DFT, HOMO, LUMO, corrosion inhibition, quantum computational method*

INTRODUCTION

The electron-donating and nitrogen atoms act as corrosion inhibitors in organic compounds such as oxadiazole, imidazole ring, and polymer molecules [1]. By attaching different electron-donating functional groups and cyclic compounds, some researchers were able to construct fairly potent inhibitor molecules to prevent metal corrosion [2–4]. Fig. 1 shows some of them as well because of electron-donating functional groups and the conjugation of π-bonds present in benzene rings in their molecular structures, such organic cyclic molecules pump more electrons to the metal surface [5]. Metal corrosion, an undesirable action, is responsible for significant economic losses globally due to the degradation of metal surfaces. Iron is one of these metals, and it is regarded as the backbone of modern industriousness [6]. Corrosion inhibitors routinely used in acidic solutions are frequently utilized to protect ferrous surfaces from corrosion [7]. The last few decades have seen significant advances in corrosion investigations, especially in the synthesis and engineering of novel corrosion inhibitors in material and commercial chemistry that function by adsorbing on the metal surface [8]. Organic molecules that can contribute electrons to the metal surface's vacant *d*-orbitals to make coordinate covalent bonds and absorb free electrons from the metal surface by exploiting their anti-bond orbitals to produce feedback bonds are good corrosion preventive [9, 10]. Studies discovered that adsorption on the surface of a metal is mostly determined by the inhibitor group's physicochemical qualities, such as the electronic density, functional group at the *p*-orbital character and donor atom [11–16]. Molecules' corrosion inhibition performances are intimately connected to their structural configurations. It is generally known that compounds having a larger quantity of heteroatoms with a π-conjugated heterocyclic system are more efficient corrosion inhibitors than compounds with merely an aliphatic chain in their chemical structures [17]. The organic electronic configuration includes several adsorptions due to high energy, also including O, S, and N atoms, as well as the molecular size, construction of metallic compounds, mode of adsorption and the projected area of the inhibitor on the metallic surface (degree of surface coverage), all influence inhibition efficiency [18–20].

In this paper, we discuss the structure and some important parameters of each molecule of BIA, HBT, MBI and PIZ calculated based on DFT and Monte Carlo simulation. Previous

studies have shown which of these identified materials have the highest and lowest levels of corrosion, but this study theoretically finds the same result.

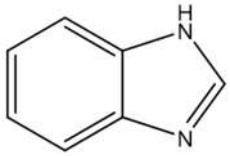

BIA
a

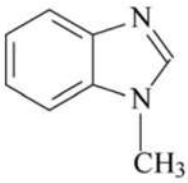

MBI
c

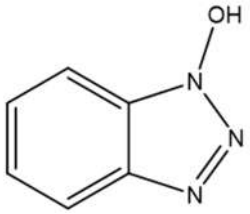

HBT
b

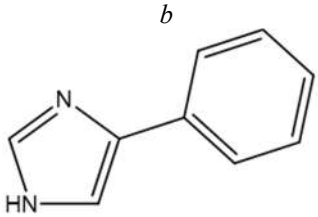

PIZ
d

Fig. 1. Chemical structures of selected compounds

QUANTUM CHEMICAL PARAMETERS

DFT calculations were performed using the Becke three-parameter nonlocal exchange functional with Lee and Miehlich's nonlocal correlation, as well as the conventional double-zeta plus polarization 6-311++G(d,p) basis set implemented in the Gaussian09 software package [21]. The computation will be referred to as B3LYP/6-311++G(d,p) following conventional nomenclature [2, 22]. The geometry of the chemical under examination was found by optimizing all geometrical variables without regard for symmetry.

Among the most prominent theoretical model used in describing materials and chemistry is the density functional theory (DFT). Various chemical principles have been linked inside the DFT system. The electron density (r), representing all chemical values which are represented, is the most crucial requirement in DFT [23]. The structural parameters computed using the (r) concept look good compared to the values derived using the idea. Because this theory is easier than quantum theory, there is a growing interest in utilizing DFT to explain the structure, characteristics, reactivity, and dynamics of atoms, molecules, and clusters. DFT transcends the limit of wave mechanics in the field of reaction chemistry, and it is developing as a distinct technique for studying reaction mechanisms [24].

This study calculated the energy of the highest occupied molecular orbital (E_{HOMO}), the energy of the lowest unoccupied molecular orbital (E_{LUMO}), ionization potential (I), electrophilicity, nucleophilicity, absolute hardness, electron affinity (A), absolute electronegativity (χ), back donation energy, and the efficiencies of corrosion inhibitors. The E_{HOMO} and E_{LUMO} may be used to describe the ionization potential (I), electron affinity (A), dipole moment, total energy, electronegativity (χ), and global hardness (σ) according to Koopman's theorem, which underpins the interpretation of these parameters. From the following equation one can calculate the ionization potential and is the energy directed to remove an electron from a molecule [25]:

$$I = -E_{HOMO}. \quad (1)$$

The energy produced when a proton is introduced to a system is characterized as electron affinity (A). It is associated with ELUMO via the following expression:

$$A = -E_{LUMO}. \quad (2)$$

Electronegativity is a description of an atom's or group of atoms' ability to pull electrons radially outward [26]; it may be computed using Formula (3):

$$\chi = \frac{I+A}{2}. \quad (3)$$

Chemical hardness is denoted by (η) is a characteristic of an atom's resistance to charge transfer [27] that may be calculated by using this formula:

$$\eta = \frac{I-A}{2}. \quad (4)$$

RESULTS AND DISCUSSION

Frontier molecular orbitals. Electrical charges in the compound were clearly the main driver of electrostatic interactions, and it has been found that local electron concentrations or charges are crucial in many chemical processes and physicochemical features of substances [28]. The highest occupied molecular orbital energy (E_{HOMO}) and lowest unoccupied molecular orbital energy (E_{LUMO}) are two of the most often used quantum chemistry characteristics. These orbitals, also known as border orbitals, govern how a molecule interacts with other species. Because it is the outermost (highest energy) orbital carrying electrons, the HOMO might operate as an electron donor. Because it is the outermost (lowest energy) orbital with space to take electrons, the LUMO is the orbital that might operate as an electron acceptor [29]. The production of a transition state is caused by an interaction between the reactants' frontier orbitals, according to the frontier molecular orbital theory. The HOMO energy is proportional to the ionization potential, while the LUMO energy is proportional to the electron affinity. The HOMO-LUMO gap, or the difference in energy between the HOMO and LUMO, is a key indicator of stability. A significant HOMO-LUMO gap indicates that the molecule will be stable in chemical processes. The HOMO-LUMO energy gap has also been used to establish the idea of activation hardness [30]. The qualitative concept of hardness is directly connected to polarizability since a smaller energy gap generally results in simpler polarization of the molecule. According to the quantum chemical calculations in this work, when the length rose [31], the HOMO energy level climbed intensely while the energy gap decreased rapidly. The linear link between MO energy level and corrosion inhibition efficiency (Fig. 2 *a*, *b*) demonstrated that the higher the inhibitor's HOMO energy, the greater the tendency of supplying electrons to the metal's vacant *d* orbital.

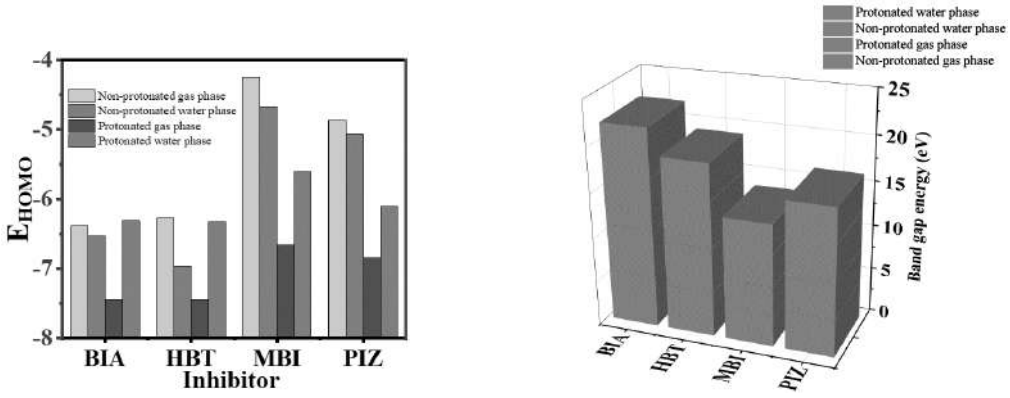

a *b*

Fig. 2. (*a*) the variation of E_{HOMO} and (*b*) the bandgap energy of selected molecules in gas and aqueous phase

The inhibitory action of the inhibitor chemical is generally attributed to molecule adsorption on the metal surface. According to the adsorption intensity, there might be physical adsorption (physisorption) or chemical adsorption (chemisorption) [32]. When chemical adsorption occurs, one of the interacting species serves as an electron pair donor, while another serves as an electron pair acceptor. When E_{HOMO} is high, the compound has a proclivity to give electrons to suitable molecules with low energy, and unoccupied *d*-orbitals. By affecting the transport process through into the adsorbed layer, increased E_{HOMO} levels accelerate adsorption and improve inhibitory efficiency [33]. As a result, larger E_{HOMO} values suggest a stronger inclination toward electron donation, promoting inhibitor adsorption on mild steel and improving inhibition

efficacy. E_{LUMO} denotes the molecule's capacity to take electrons. In this study, we completed calculations about all the molecules identified on this basis of the E_{HOMO} order as D>C>A>B, as shown in Tables 1 to 4, which is exactly similar to the practical results for the level of corrosion inhibition.

The energy gap (ΔE) is an important property without theoretically addressing the issue of corrosion inhibition, which is the response of the inhibitor molecule to adsorption on the metal surface. The reactivity of the molecules decreases as the band gap energy increases and *vice versa*. Poor corrosion inhibitors are known to have high energy gap values [34]. This is due in itself to the fact that the ionization energy required to remove an electron from the last occupied orbit is maximal. Organic compounds that not only donate electrons to the vacant orbital of the metal but also take free electrons from the metal are often excellent corrosion inhibitors. Molecule C has the lowest value in terms of band gap energy and indicates the fact that it has the highest level of corrosion inhibition, and molecule B has the highest bandgap, indicates the worst inhibitor of corrosion, which is entirely consistent with the practical results. So the use of this approach is correct.

Dipole moment. The dipoles moment of the neutral and protonated inhibitors in the gas and aqueous phases were estimated, as shown in Tables 1 to 4. The larger the dipole moment, the more important it becomes, and the stronger the intermolecular interactions, resulting in the formation of highly adsorbed layers on the metal surface [35]. The dipole moments may be used to predict the complete surface coverage of inhibitors on the Fe surface. When molecules with a strong dipole moment, which increases their resistance to corrosion, are adsorbed on a metal surface, they have significant coverage, and increases the corrosion inhibition effect of these compounds. An increase in the value of the dipole moment causes an increase in polarization, where electrons are easily transferred from a high level to a suitable lower level in an empty orbital [36]. The softness of organic materials can also be determined by the dipole moment because the inhibitor with a high value of dipole moment also has a high value of softness and the highest adsorption occurs in areas of high softness, which increases the inhibition corrosion efficiency. The ranking for corrosion levels of all inhibitors is D >C > A > B, which is exactly the same as the practical results.

Ionization potential and electronegativity. The ionization potential (I) can be an important parameter for determining the interaction of atoms or molecules. High levels of ionization potential suggest that compounds are very reactive, playing a major role in terms of activity and inactivity of chemical reactions, for example, while low values of ionization potential indicate that molecules are inactive [2, 37, 38]. Tables 1 and 4 show an increase in ionizability, which corresponds to an increasing trend of E_{HOMO}.

The low electronegativity value characterizes an excellent corrosion inhibitor. The results in Tables 1–4 show that the electronegative order follows the D < C < A <B trend, which is consistent with the experimental data B < A < C < D, increases. According to Sanderson's electronegativity matching concept, D is predicted by low electronegativity and high difference in electronegativity, molecule B has the most electronegativity and that indicates the worst inhibitor which indicates small inhibition efficiency. The same idea may be applied to chemical potential.

Hardness and softness. Absolute hardness and softness are one of the two main objectives of this study and related to many other properties when studying the structure of matter, known properties used to assess the stability and interaction of molecules [39]. Some of the properties associated with the absolute hardness value that it exhibits under low chemical reaction disturbances include the resistance to deformation or polarization of the electron cloud of atoms, ions, or molecules [40]. Hard molecules have exactly different properties from substances with high absolute permeability. For example, hardest substances have a large energy gap, while soft molecules have a small energy gap. Consequently, molecules with the lowest global hardness values are predicted to be excellent corrosion inhibitors as demonstrated in this study for noble metals under acidic conditions. Adsorption of an inhibitor onto a metallic surface occurs at the softest and least the hard part of a molecule. Tables 1 to 4 show the hardness and softness values of all the identified molecules with the basis set of 6-311++G(d,p) in protonated and unprotonated species for both gas and aqueous phase. These calculations showed that molecule C has the lowest hardness of all other

molecules and molecule B has the highest as shown in Fig. 3 *a*, *b*. On this basis, we can conclude that molecule C has the highest corrosion inhibition, because it has been proven in all previous studies that the highest softness indicates the best inhibitor of corrosion.

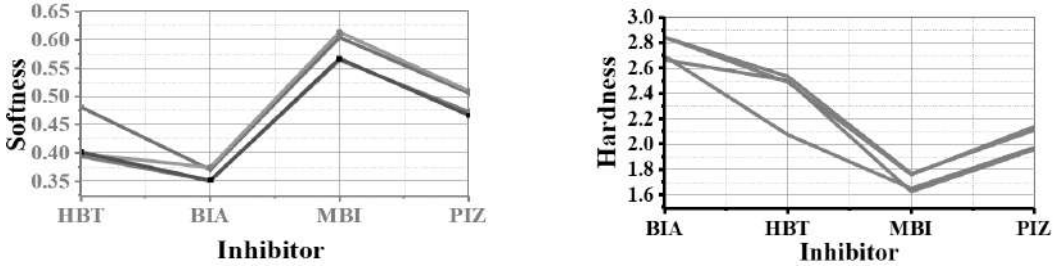

a *b*

Fig. 3. (*a*) variation of softness and (*b*) variation of hardness of selected molecules based on DFT calculation at 6-311++G(d,p) basis set in protonated and non-protonated species of gas and aqueous phases

Electrophilicity and nucleophilicity. The electrophilic attack refers to the regions that are most capable of absorbing electrons to form feedback bonds with the Fe surface [41]. This is also consistent with the calculated LUMO spin density, and is supported by local two-scale electrophilicity and nucleophilicity values, and shows that these inhibitors have active sites matching most other parameters. Knowing each of the nucleophilicity values and the high value suggests a tendency to donate electrons to unoccupied nuclear orbitals on the iron surface, resulting in the formation of a coordinate bond [42]. The electrostatic attack values indicate that these are the sites with the greatest potential to absorb electrons to form feedback bonds with the Fe surface. This is also consistent with the estimated LUMO spin density and confirmed by local binary measures.

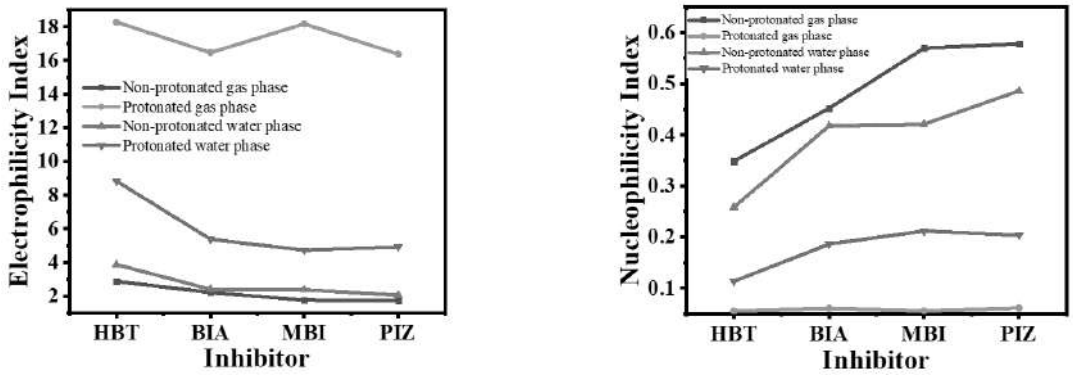

a *b*

Fig. 4. The order of electrophilicity index (*a*) and order of nucleophilicity index (*b*) of the inhibitors

As explained in Fig. 4 *a*, *b* for the electrophilicity and nucleophilicity of all inhibitors, the best corrosion inhibitor molecule C has the highest value in electrophilicity, indicating that it is the best molecule for electron donation.

Electron transfer. When iron and a corrosion inhibitor come close, a chemical process occurs in which electrons flow from below (inhibitor) to higher (iron), until their chemical ($\boldsymbol{\eta}$) or electronegative ($\boldsymbol{\chi}$) potentials are equal [41].

$$\Delta N_{max} = \frac{\chi_{Fe} - \chi_{inh}}{2(\eta_{Fe} + \eta_{inh})}. \qquad (5)$$

The role of hardness is to create a barrier to the transfer of the electron, but the difference in electronegativity is that it promotes the transfer of electrons. Consequently, we can calculate for the passage of the number of electrons, a theoretical

value for the electronegativity of bulk iron, χ_{Fe} = 7 eV, and the global hardness η_{Fe} = 0, were used, assuming that for a metallic bulk $I = A$ since they are softer than neutral metal atoms [43]. Through this parameter, we can determine which inhibitors are electron donors and which are electron acceptors. If the number of transferred electrons is less than 3.6, it is increasing the electron donation on the metal surface, and the inhibitor has also enhanced the ability to inhibit corrosion. In this study, we found that the MBI inhibitor is the best because the maximum number of electrons occurred in the non-protonated state, 1.27 and 1.15 in the gas and aqueous phases, respectively.

Back - donation energy. Another important parameter related to the corrosion level of materials and according to a model that can be interpreted for charge transfer to donation and chargeback donation suggested that the interaction between the inhibitor molecule and the metal surface governs the electronic back donation process [44]. Based on this concept, the time for back donation and electron transfer to the molecule is the same, we can calculate this by using a relationship to the hardness of the inhibitor, and the change in energy is directly proportional to the hardness of the molecule:

$$\Delta E_{back-donation} = -\frac{\eta}{4}. \quad (6)$$

Back donation from the molecule to the metal is energetically advantageous, this occurs when the stiffness is greater than zero and the back donation from the molecule to the metal is less than zero. The back donation is less than zero in all the different cases and the stiffness is all greater than zero, which means that the back donation from the molecule to the metal is energetically favorable as shown in Tables 1 to 4. Through a proper interpretation of this, we can define that the inhibition efficiency increases as the molecule adsorbs more actively on the metal surface, leading to an increase in inhibition efficiency when the stabilization energy released from the interaction between the metal surface and the inhibitor increases. Figs. 5 and 6 show the results of the materials used in this study. Fig. 5 shows the HOMO and LUMO, and Fig. 6 shows the electrostatic potential map and optimization of the molecules.

Table 1. Quantum chemical parameters of BIA

Quantum chemical parameters	Gas phase		Aqueous phase	
	Non-protonated gas phase	Protonated gas phase	Non-protonated water phase	Protonated water phase
HOMO	-6.388	-12.0367	-6.5332	-8.0807
LUMO	-0.7037	-6.7035	-0.8471	-2.6885
Dipole moment (a.u)	1.446E+00	1.471E+00	1.979E+00	1.972E+00
Total energy (eV)	-1.034E+04	-1.033E+04	-1.034E+04	-1.033E+04
Ionization energy	6.388	12.0367	6.5332	8.0807
Electron affinity	0.7037	6.7035	0.8471	2.6885
Energy gap	5.6843	5.3332	5.6861	5.3922
Hardness	2.84215	2.6666	2.84305	2.6961
Softness	0.351846314	0.375009375	0.351734933	0.370906124
Electronegativity	3.54585	9.3701	3.69015	5.3846
Chemical potential	-3.54585	-9.3701	-3.69015	-5.3846
Electrophilicity	2.211891037	16.46268169	2.394823697	5.377010712
Nucleophilicity	0.452101836	0.060743445	0.417567273	0.18597694
Back-donation	-0.7105375	-0.66665	-0.7107625	-0.674025
Electron transfer	0.607664972	-0.44440486	0.582094933	0.299580876
Initial molecule $\Delta\psi$	-1.049482981	-0.526641979	-0.963323457	-0.241971474

Table 2. Quantum chemical parameters of HBT

Quantum chemical parameters	Gas phase		Aqueous phase	
	Non-protonated gas phase	Protonated gas phase	Non-protonated water phase	Protonated water phase
HOMO	-6.2711	-12.0658	-6.9639	-8.1294
LUMO	-1.2916	-7.0605	-1.8955	-3.9783
Dipole moment (a.u)	1.509E+00	1.677E+00	2.335E+00	8.857E-01
Total energy (eV)	-1.282E+04	-1.281E+04	-1.282E+04	-1.281E+04
Ionization energy	6.2711	12.0658	6.9639	8.1294
Electron Affinity	1.2916	7.0605	1.8955	3.9783
Energy gap	4.9795	5.0053	5.0684	4.1511
Hardness	2.48975	2.50265	2.5342	2.07555
Softness	0.401647	0.399576	0.394601847	0.4818
Electronegativity	3.78135	9.56315	4.4297	6.05385
Chemical potential	-3.78135	-9.56315	-4.4297	-6.05385
Electrophilicity	2.871495	18.2714	3.871486483	8.828768
Nucleophilicity	0.348251	0.05473	0.258298719	0.113266
Back-donation	-0.62244	-0.62566	-0.63355	-0.51889
Electron transfer	0.64638	-0.51209	0.507122563	0.227928
Initial molecule $\Delta\psi$	-1.04024	-0.65628	-0.651728562	-0.10783

Table 3. Quantum chemical parameters of MBI

Quantum chemical parameters	Gas phase		Aqueous phase	
	Non-protonated gas phase	Protonated gas phase	Non-protonated water phase	Protonated water phase
HOMO	-4.25073	-9.32184	-4.67277	-5.60694
LUMO	-0.7252	-6.0646	-1.13091	-2.29936
Dipole moment (a.u)	9.036E-01	8.695E-01	2.102E+00	1.238E+00
Total energy (eV)	-2.117E+04	-2.116E+04	-2.117E+04	-2.117E+04
Ionization energy	4.25073	9.32184	4.67277	5.60694
Electron Affinity	0.7252	6.0646	1.13091	2.29936
Energy gap	3.52553	3.25724	3.54186	3.30758
Hardness	1.762765	1.62862	1.77093	1.65379
Softness	0.567291	0.614017	0.564675	0.604672
Electronegativity	2.487965	7.69322	2.90184	3.95315
Chemical potential	-2.48797	-7.69322	-2.90184	-3.95315
Electrophilicity	1.755756	18.17049	2.377473	4.724722
Nucleophilicity	0.569555	0.055034	0.420615	0.211653
Back-donation	-0.44069	-0.40716	-0.44273	-0.41345
Electron transfer	1.279818	-0.21282	1.157064	0.921172
Initial molecule $\Delta\psi$	-2.88729	-0.07377	-2.37092	-1.40334

Table 4. Quantum chemical parameters of PIZ

Quantum chemical parameters	Gas phase		Aqueous phase	
	Non-protonated gas phase	Protonated gas phase	Non-protonated water phase	Protonated water phase
HOMO	-4.86215	-9.97625	-5.0605	-7.38272
LUMO	-0.57933	-6.05399	-0.83457	-2.43242
Dipole moment (a.u)	1.598E+00	1.697E+00	2.158E+00	2.598E+00
Total energy (eV)	-1.244E+04	-1.244E+04	-1.244E+04	-1.244E+04
Ionization energy	4.86215	9.97625	5.0605	6.38272
Electron Affinity	0.57933	6.05399	0.83457	2.43242
Energy gap	4.28282	3.92226	4.22593	3.9503
Hardness	2.14141	1.96113	2.112965	1.97515
Softness	0.466982	0.50991	0.473269	0.506291
Electronegativity	2.72074	8.01512	2.947535	4.40757
Chemical potential	-2.72074	-8.01512	-2.94754	-4.40757
Electrophilicity	1.7284	16.37886	2.05587	4.917772
Nucleophilicity	0.57857	0.061054	0.486412	0.203344
Back-donation	-0.53535	-0.49028	-0.52824	-0.49379
Electron transfer	0.999169	-0.25881	0.958952	0.656262
Initial molecule $\Delta\psi$	-2.13785	-0.13136	-1.94306	-0.85066

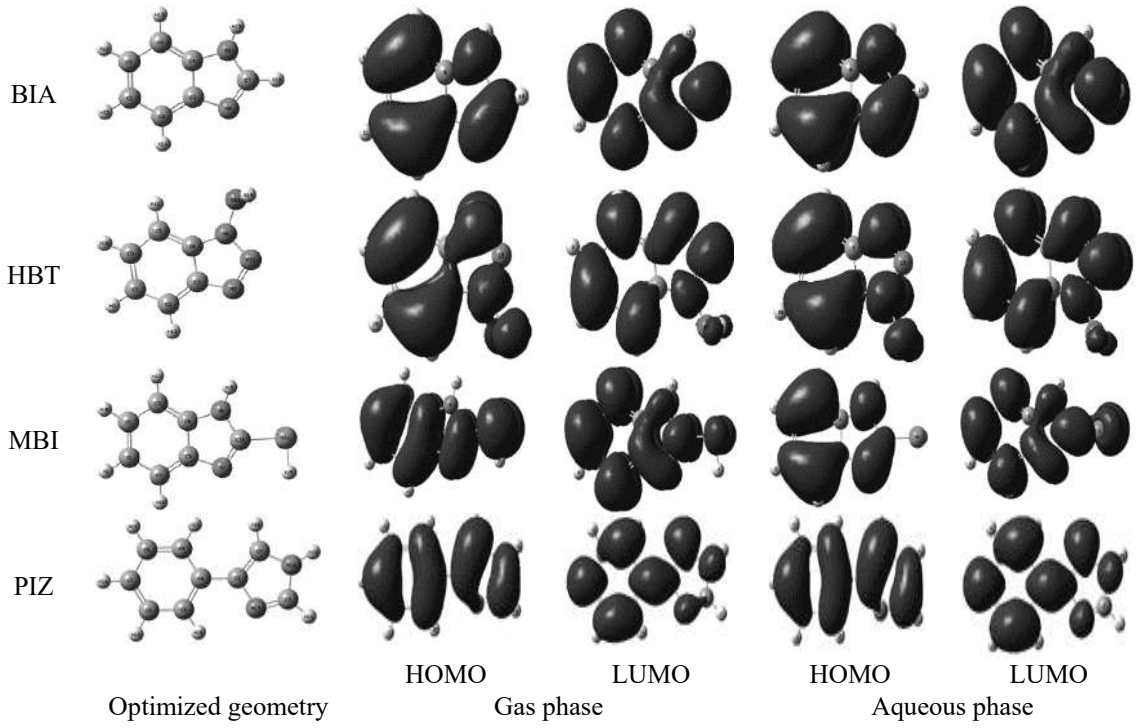

Fig. 5. Optimized geometry, HOMO and LUMO of the molecules

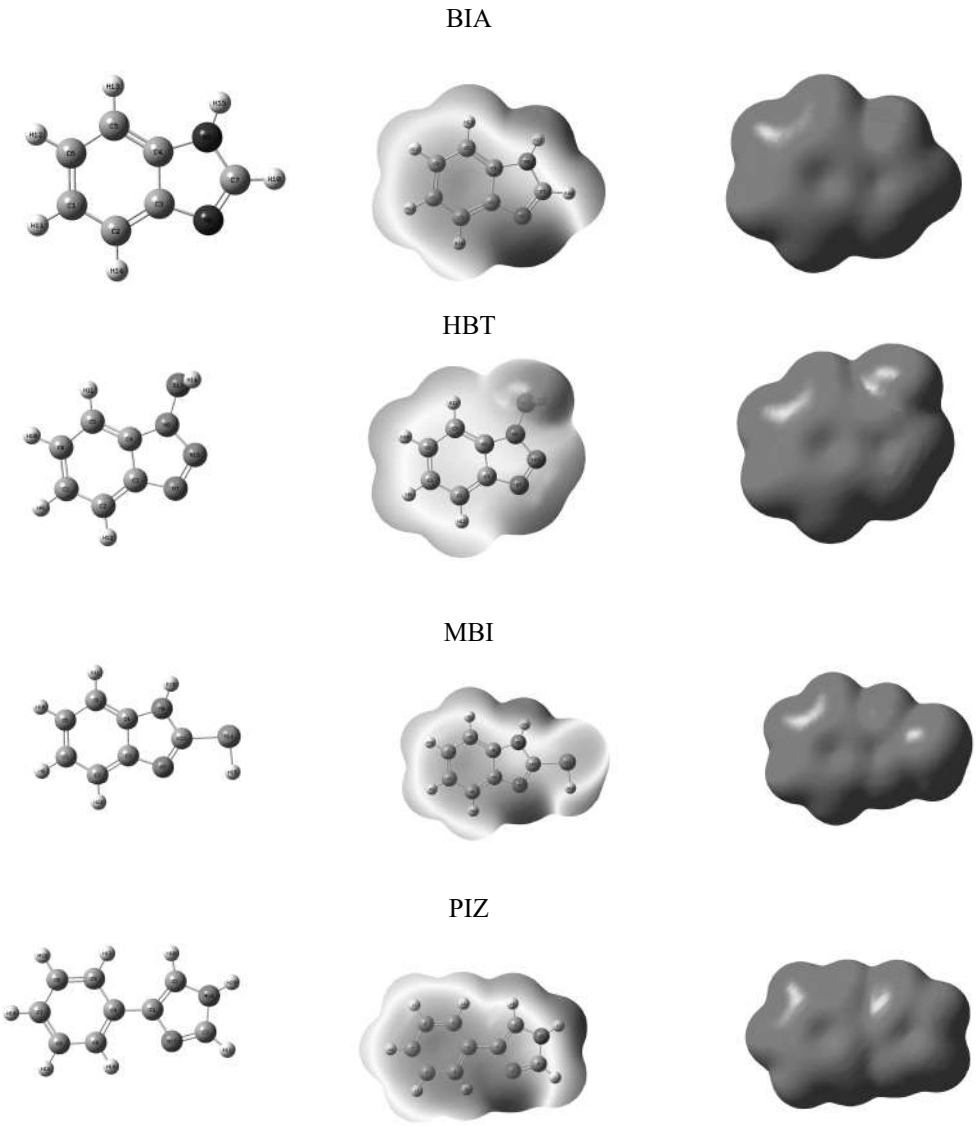

Fig. 6. Molecular structures and electrostatic potential maps

Monte Carlo simulation. The adsorption process of four selected inhibitors on a clean Fe surface is examined using Monte Carlo simulations performed with cutting-edge software called Material Studio 7.0 [45]. Because it is the most stable surface documented in the literature, the Fe (110) crystal surface was chosen for this simulation. A four-slab model was used to simulate the Fe (110) surface. Each layer in this model had 80 iron atoms, representing a (110) unit cell. For no bonded interactions, a cut-off distance of 1.85 nm used with a spline transformation function (total energy, average total energy, van der Waals, electrostatic interactions, and intramolecular energy). A low-energy adsorption site calculated by performing a Monte Carlo search of the structure space of the substrate-adsorbed system while gradually reducing the temperature (simulated heating). This repeatable procedure is one of the successful methods to find more local minimum energy. The adsorbed molecules rotate randomly and are translated around the substrate during the simulation. Based on the Metropolis Monte Carlo method selection principles accept or reject the structure that emerges in one of these phases areused.

The typical energy configuration for all molecules were found as shown in Fig. 7. They were total energy, average total energy, van der

Waals energy, electrostatic energy and intramolecular energy. The stimulation experiment was performed on iron (110), and a set of chemical and physical properties were obtained as shown in Table 5. The adsorption energy, is attributed to the energy produced while the relaxed adsorption components deposit on the substrate. The adsorption energy can be defined as the sum of the energies of solid adsorption and the deformation of the adsorbent molecule. Higher negative adsorption energy values are clear indicators of a more stable and higher interaction between a metal and an inhibitor molecule. Table 5 shows that the negative values of the adsorption energies of the derivatives of all the inhibitors on the Fe (110) surface are as follows the order C > D > A > B. The maximum amount of negative adsorption energy indicates the highest inhibitor.

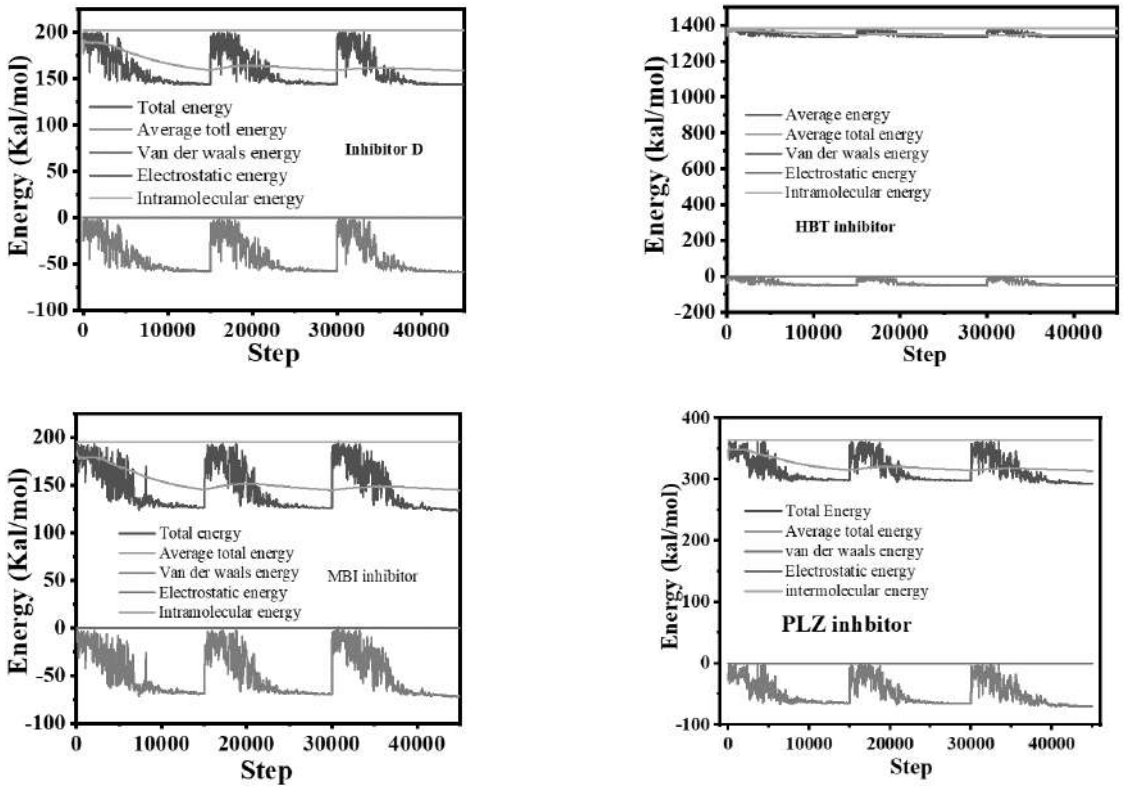

Fig. 7. Typical energy profile on Fe (110) based on Monte Carlo simulation

Table 5. The outputs and descriptors calculated by the Monte Carlo simulation for adsorption of selected inhibitors on Fe (110) (in kcal mol^{-1}) and experimental inhibition efficiency [46, 47]

Inhibitor	Total energy	Adsorption energy	Rigid adsorption	Deformation energy	dE_{ad}/dN_i	Experi-mental efficiency
BIA	144.26004346	-57.97798243	-57.97798243	-2.305313e-009	-57.97798243	86
HBT	1.331356e+003	-51.04817159	-51.04817160	7.501285e-009	-51.04817159	82
MBI	127.67217704	-67.79102470	-67.79102470	-2.066258e-011	-67.79102470	99
PLZ	296.70896331	-66.99585942	-66.99585942	-2.025899e-010	-66.99585942	95.84

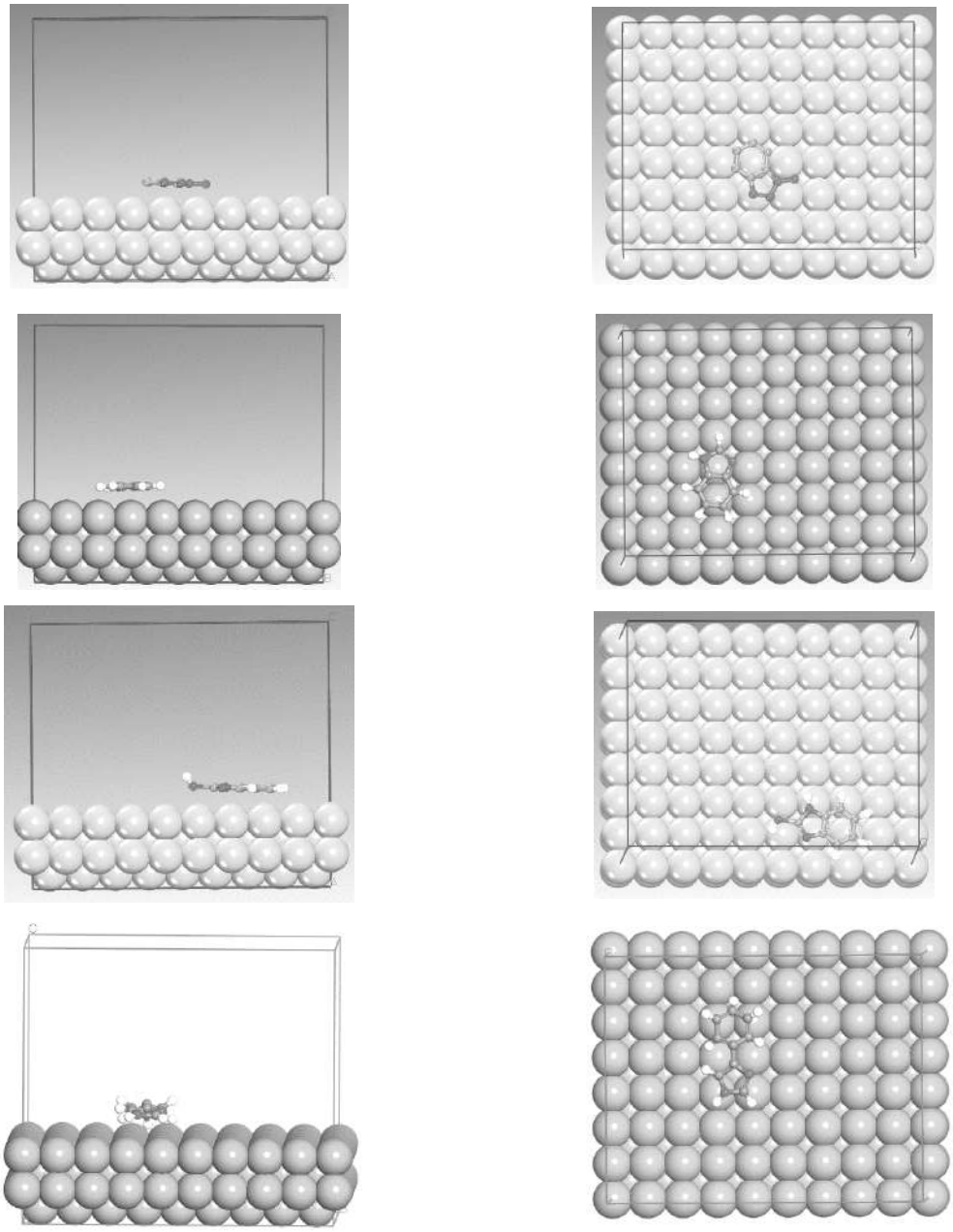

Fig. 8. Top view and side view of Monte Carlo simulation at most stable low energy configuration for adsorption on Fe (110) surface

CONCLUSIONS

The level of inhibition of each A, B, C, and D molecule was determined according to a number of important parameters, including HOMO, LUMO, Global hardness and softness. In order to study the structure of the material and discover its important properties related to electron motion, DFT can be used. Additionally, it is relatively easy to find the root cause in terms of structure and composition to match the experimental data. The highest softness value indicated the best inhibitor, whereas the hardest material indicated the worst molecule in this study. One of the significant parameters was polarization. Due to this factor, each molecule's corrosion levels could be ranked. According to Monte Carlo, the corrosion inhibitor with the highest negative value will be the one with the highest adsorption energy, which is in a way the same result as the practical one. C > D > A > B is the corrosion prevention efficiency rating.

Квантові обчислення та теорія функціоналу густини щодо ефективності інгібування корозії сполуками BIA, HBT, MBI та PIZ

Д.М. Маманд, Х.М. Кадр

Університет Рапаріна, науковий коледж, кафедра фізики
Сулейманія, 46012, Ірак, hiwa.physics@uor.edu.krd

Це дослідження визначило рівні інгібування корозії молекулами бензімідазолу (BIA), 1-гідроксибензотриазолу (HBT), метилбензімідазолу (MBI) і 4-фенілімідазолу (PIZ). Використовуючи моделювання, можна було мати повний зв'язок з експериментальною роботою, оскільки результати були повністю узгодженими. Теорія функціоналу густини (DFT) і моделювання методом Монте-Карло були використані для розрахунку кількох квантовохімічних параметрів. Молекули розраховуються методами квантової хімії, за допомогою програмного забезпечення Gaussian09. Фундаментальними факторами, що визначають порядок корозії молекул, є зайняті молекулярні орбіталі з найвищою енергією та незайняті молекулярні орбіталі з найнижчою енергією (HOMO та LUMO), енергія граничних молекулярних орбіт, енергія зворотного донорства, електрофільність, нуклеофільність, енергетична щілина ΔE, абсолютна електронегативність (χ), м'якість, число електронів (ΔN), що переносяться від інгібіторів до заліза, дипольний момент (μ), глобальна твердість (η) і повна енергія.

***Ключові слова**: DFT, HOMO, LUMO, інгібування корозії, квантовий обчислювальний метод*

REFERENCES

1. Marinescu M. Recent advances in the use of benzimidazoles as corrosion inhibitors. *BMC Chem*. 2019. **13**(1): 1.
2. Mamand D. Theoretical calculations and spectroscopic analysis of gaussian computational examination-NMR, FTIR, UV-Visible, MEP on 2, 4, 6-Nitrophenol. *Journal of Physical Chemistry and Functional Materials*. 2019. **2**(2): 77.
3. Qadr H.M., Mamand D.M. Molecular structure and density functional theory investigation corrosion inhibitors of some oxadiazoles. *J. Bio- Tribo-Corros.* 2021. **7**(4): 1.
4. Qadr H.M. Pressure effects on stopping power of alpha particles in argon gas. *Phys. Part. Nucl. Lett.* 2021. **18**(2): 185.
5. Wu Z., Liu Q., Yang P., Chen H., Zhang Q., Li S., Tang Y., Zhang S. Molecular and Morphological Engineering of Organic Electrode Materials for Electrochemical Energy Storage. *Electrochem. Energy Rev.* 2022. **5**(1): 1.
6. Hull G. The excavation and analysis of an 18th-century deposit of anatomical remains and chemical apparatus from the rear of the first Ashmolean Museum (now The Museum of the History of Science), Broad Street, Oxford. *Post-Medieval Archaeol.* 2003. **37**(1): 1.
7. Ansari F.A., Verma C., Siddiqui Y.S., Ebenso E.E., Quraishi M.A. Volatile corrosion inhibitors for ferrous and non-ferrous metals and alloys: A review. *International Journal of Corrosion and Scale Inhibition*. 2018. **7**(2): 126.
8. Umoren S.A., Solomon M.M. Recent developments on the use of polymers as corrosion inhibitors-a review. *The Open Materials Science Journal*. 2014. **8**(1): 39.
9. Mamand D.M., Awla A.H., Anwer T.M.K., Qadr H.M. Quantum chemical study of heterocyclic organic compounds on the corrosion inhibition. *Chimica Techno Acta*. 2022. **9**(2): 20229203.
10. Mamand D.M., Rasul H.H., Omer P.K., Qadr H.M. Theoretical and experimental investigation on ADT organic semiconductor in different solvents. *Condensed Matter and Interphases*. 2022. **24**(2): 227.
11. Lesar A., Milošev I. Density functional study of the corrosion inhibition properties of 1, 2, 4-triazole and its amino derivatives. *Chem. Phys. Lett*. 2009. **483**(4–6): 198.
12. Ebenso E.E., Arslan T., Kandemirlı F., Love I., Öğretır C.l., Saracoğlu M., Umoren S.A. Theoretical studies of some sulphonamides as corrosion inhibitors for mild steel in acidic medium. *Int. J. Quantum Chem.* 2010. **110**(14): 2614.
13. Qadr H.M. Effect of ion irradiation on the hardness properties of Zirconium alloy. *Annals of the University of Craiova, Physics*. 2019. **29**: 68.

14. Qadr H.M. Effect of ion irradiation on the mechanical properties of high and low copper. *Atom Indonesia*. 2020. **46**(1): 47.
15. Qadr H.M. A molecular dynamics calculation to cascade damage processes. *The Annals of "Dunarea de Jos" University of Galati. Fascicle IX, Metallurgy and Materials Science*. 2020. **43**(4): 13.
16. Qadr H.M. Radiation damage and dpa in iron using mcnp5. *European J. Mater. Sci. Eng*. 2020. **5**(3): 109.
17. Assad H., Kumar A. Understanding functional group effect on corrosion inhibition efficiency of selected organic compounds. *J. Mol. Liq*. 2021. **344**: 117755.
18. Umoren S., Solomon M. Effect of halide ions on the corrosion inhibition efficiency of different organic species–A review. *J. Ind. Eng. Chem*. 2015. **21**: 81.
19. Ahmed S.K., Ali W.B., Khadom A.A. Synthesis and investigations of heterocyclic compounds as corrosion inhibitors for mild steel in hydrochloric acid. *Int. J. Ind. Chem*. 2019. **10**(2): 159.
20. Qadr H.M. A molecular dynamics study of temperature dependence of the primary state of cascade damage processes. *Russ. J. Non-Ferrous Met.* 2021. **62**(5): 561.
21. Frisch A.J.W., USA, 25p gaussian 09W Reference. 2009. **470**.
22. Mamand D.M., Qadr H.M. Comprehensive spectroscopic and optoelectronic properties of bbl organic semiconductor. *Prot. Met. Phys. Chem*. 2021. **57**(5): 943.
23. Domingo L.R., Ríos-Gutiérrez M., Pérez P. Applications of the conceptual density functional theory indices to organic chemistry reactivity. *Molecules*. 2016. **21**(6): 748.
24. Mamand D. Determination the band gap energy of poly benzimidazobenzophenanthroline and comparison between HF and DFT for three different basis sets. *Journal of Physical Chemistry and Functional Materials*. 2019. **2**(1): 32.
25. Bulat F.A., Toro-Labbé A., Brinck T., Murray J.S., Politzer P. Quantitative analysis of molecular surfaces: areas, volumes, electrostatic potentials and average local ionization energies. *J. Mol. Model*. 2010. **16**(11): 1679.
26. Mamand D.M., Anwer T.M., Qadr H.M., Mussa C.H. Investigation of Spectroscopic and Optoelectronic Properties of Phthalocyanine Molecules. *Russ. J. Gen. Chem*. 2022. **92**(9): 1827.
27. V Putz M. Electronegativity and chemical hardness: different patterns in quantum chemistry. *Current Physical Chemistry*. 2011. **1**(2): 111.
28. Achak M., Hafidi A., Ouazzani N., Sayadi S., Mandi L. Low cost biosorbent "banana peel" for the removal of phenolic compounds from olive mill wastewater: Kinetic and equilibrium studies. *J. Hazard. Mater*. 2009. **166**(1): 117.
29. Junaedi S., Kadhum A.A.H., Al-Amiery A.A., Mohamad A.B., Takriff M.S. Synthesis and characterization of novel corrosion inhibitor derived from oleic acid: 2-Amino 5-Oleyl-1, 3, 4-Thiadiazol (AOT). *Int. J. Electrochem. Sci*. 2012. **7**(4): 3543.
30. Li L., Cai T., Wang Z., Zhou Z., Geng Y., Sun T. Study on molecular structure, spectroscopic investigation (IR, Raman and NMR), vibrational assignments and HOMO–LUMO analysis of L-sodium folinate using DFT: A combined experimental and quantum chemical approach. *Spectrochim. Acta, Part A*. 2014. **120**: 106.
31. Gece G., Bilgiç S. A theoretical study on the inhibition efficiencies of some amino acids as corrosion inhibitors of nickel. *Corros. Sci*. 2010. **52**(10): 3435.
32. Popova A., Christov M., Deligeorgiev T. Influence of the molecular structure on the inhibitor properties of benzimidazole derivatives on mild steel corrosion in 1 M hydrochloric acid. *Corrosion*. 2003. **59**(09): 03090756.
33. Obot I., Kaya S., Kaya C., Tüzün B. Density Functional Theory (DFT) modeling and Monte Carlo simulation assessment of inhibition performance of some carbohydrazide Schiff bases for steel corrosion. *Physica E*. 2016. **80**: 82.
34. Ahamad I., Prasad R., Quraishi M. Thermodynamic, electrochemical and quantum chemical investigation of some Schiff bases as corrosion inhibitors for mild steel in hydrochloric acid solutions. *Corros. Sci*. 2010. **52**(3): 933.
35. Khaled K., Babić-Samardžija K., Hackerman N. Theoretical study of the structural effects of polymethylene amines on corrosion inhibition of iron in acid solutions. *Electrochim. Acta*. 2005. **50**(12): 2515.
36. Stoyanova A., Petkova G., Peyerimhoff S. Correlation between the molecular structure and the corrosion inhibiting effect of some pyrophthalone compounds. *Chem. Phys*. 2002. **279**(1): 1.
37. Udhayakala P., Rajendiran T., Gunasekaran S. Theoretical approach to the corrosion inhibition efficiency of some pyrimidine derivatives using DFT method. *Journal of Computational Methods in Molecular Design*. 2012. **2**(1): 1.
38. Qadr H.M., Mamand D. A Review on DPA for computing radiation damage simulation. *Journal of Physical Chemistry and Functional Materials*. 2022. **5**(1): 30.
39. Parr R.G., Zhou Z. Absolute hardness: unifying concept for identifying shells and subshells in nuclei, atoms, molecules, and metallic clusters. *Acc. Chem. Res*. 1993. **26**(5): 256.

40. Hamani H., Douadi T., Daoud D., Al-Noaimi M., Rikkouh R.A., Chafaa S. 1-(4-Nitrophenylo-imino)-1-(phenylhydrazono)-propan-2-one as corrosion inhibitor for mild steel in 1 M HCl solution: weight loss, electrochemical, thermodynamic and quantum chemical studies. *J. Electroanal. Chem*. 2017. **801**: 425.
41. Khaled K. Studies of iron corrosion inhibition using chemical, electrochemical and computer simulation techniques. *Electrochim. Acta*. 2010. **55**(22): 6523.
42. Peme T., Olasunkanmi L.O., Bahadur I., Adekunle A.S., Kabanda M.M., Ebenso E.E. Adsorption and corrosion inhibition studies of some selected dyes as corrosion inhibitors for mild steel in acidic medium: gravimetric, electrochemical, quantum chemical studies and synergistic effect with iodide ions. *Molecules*. 2015. **20**(9): 16004.
43. Mamand D.M., Qadr H.M. Density Functional Theory and Computational Simulation of the Molecular Structure on Corrosion of Carbon Steel in Acidic Media of Some Amino Acids. *Russ. J. Phys. Chem. A*. 2022. **96**(10): 2155.
44. Puértolas B., Comesaña-Hermo M., Besteiro L.V., Vázquez-González M., Correa-Duarte M.A. Challenges and Opportunities for Renewable Ammonia Production via Plasmon-Assisted Photocatalysis. *Adv. Energy Mater*. 2022. **12**(18): 2103909.
45. Akkermans R.L.C., Spenley N.A., Robertson S.H. Monte Carlo methods in materials studio. *Mol. Simul*. 2013. **39**(14–15): 1153.
46. Morales-Gil P., Negrón-Silva G., Romero-Romo M., Ángeles-Chávez C., Palomar-Pardavé M. Corrosion inhibition of pipeline steel grade API 5L X52 immersed in a 1 M H_2SO_4 aqueous solution using heterocyclic organic molecules. *Electrochim. Acta*. 2004. **49**(26): 4733.
47. Yan T., Zhang S., Feng L., Qiang Y., Lu L., Fu D., Wen Y., Chen J., Li W., Tan B. Investigation of imidazole derivatives as corrosion inhibitors of copper in sulfuric acid: combination of experimental and theoretical researches. *J. Taiwan Inst. Chem. Eng.* 2020. **106**: 118.

Received 13.10.2022, accepted 05.06.2023